Electronic Supplementary Material (ESI) for Sustainable Energy & Fuels.

Supplementary information

Effective electrode design and reaction mechanism for electrochemical promotion of ammonia synthesis using Fe-based electrode catalysts

Authors: Chien-I Li, Hiroki Matsuo and Junichiro Otomo*

Affiliations and addresses:

Department of Environment Systems, Graduate School of Frontier Sciences,

The University of Tokyo,

5-1-5 Kashiwanoha, Kashiwa-shi, Chiba 277-8561, Japan

* Corresponding author:

E-mail correspondence: otomo@k.u-tokyo.ac.jp

1. TG measurement for Fe_2O_3 powder

TG-DTA measurement was performed to investigate the reduction reaction of Fe_2O_3 powder in 3%H_2. As shown in Fig. S1, the Fe_2O_3 weight was decreased by around 30% at 900°C, which corresponded to the weight loss of Fe_2O_3 reduction to Fe. The pure Fe phase was also maintained with decreasing temperature from 900°C to 550°C. The result supports that the metallic Fe phase will be maintained in the cathode catalyst at the operating temperature of around 550 °C for the electrochemical ammonia synthesis.

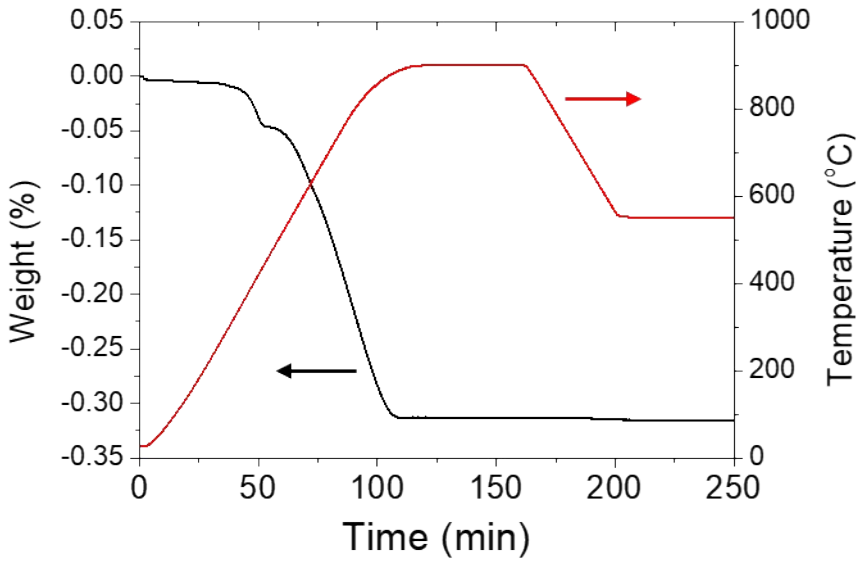

Fig. S1 Time profiles of the weight change of Fe_2O_3 powder in dry 3% H_2/Ar and temperature in the TG-DTA measurement.

2. Cross-sectional SEM images of the three types of electrodes

The cross-sectional SEM images of the three types of electrodes (type A, type A′, and type B) are shown in Fig. S2, besides Fig. 2 in the main text. The images show that the three electrodes have porous structures, and the thickness is around 15–25 μm.

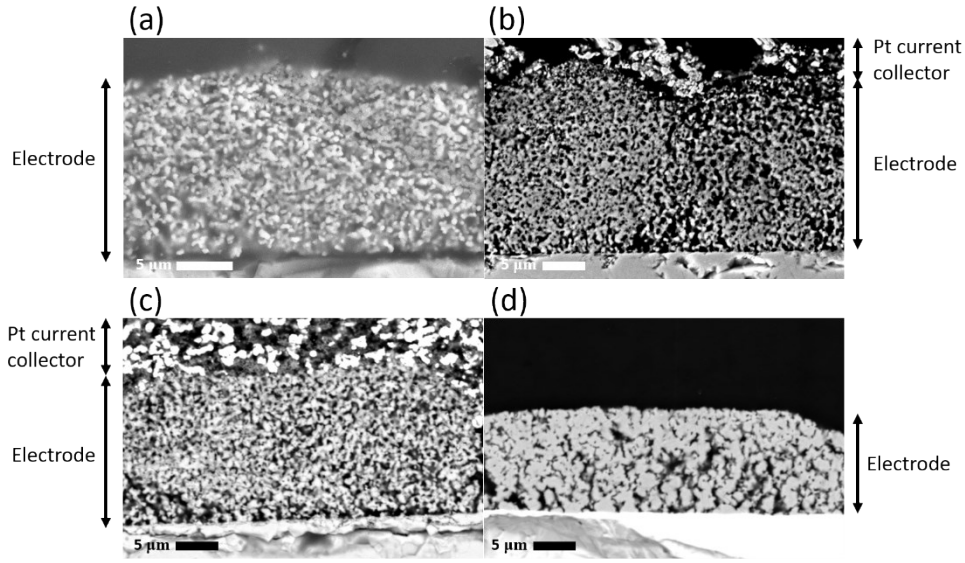

Fig. S2 Cross-sectional SEM images of (a) pure BCY, (b) 10Fe–BCY, (c) 0.5W–10Fe–BCY, and (d) porous pure Fe cathode.

3. The fraction of NH_3 formation rate to the NH_3 formation rate at equilibrium and current efficiency

Figure S3 shows the results of current efficiency, η_{CE}, and the fraction of obtained NH_3 concentration to NH_3 concentration at equilibrium, X_{Equ}, for type A, type A', and type B. The definitions of the current efficiency and X_{Equ} are described in Eqs. 12 and 13 in the main text. Type A of 10Fe–BCY cathode exhibited a current efficiency of 0.3%. Type A′ and type B showed high current efficiencies of 0.7% and 1.6%, respectively, because both cathodes had higher ammonia formation rates and lower current densities than the 10Fe–BCY cathode. X_{Equ} at 600°C increased from 0.1% to 23.0% for the type A (10Fe–BCY) cathode, from 1.1% to 25.9% for the type A′ (0.5W–10Fe–BCY) cathode, and from 0.5% to 47.4% for the type B (porous pure Fe) cathode. X_{Equ} of 0.1% – 1.1% were observed at the rest potential in the three cathodes because of the low amount of Fe catalyst and low performance of catalytic reaction under the present conditions. X_{Equ} in three cathodes increased by over 20–230 times with cathodic polarization, which demonstrated the strong electrochemical promotion. Although the ammonia formation rate obtained using type A′ (0.5W–10Fe–BCY) and type B (porous pure Fe) cathodes at 550°C was higher than that at 600°C, X_{Equ} at 550°C was lower than that at 600°C because the ammonia formation was an exothermic reaction.

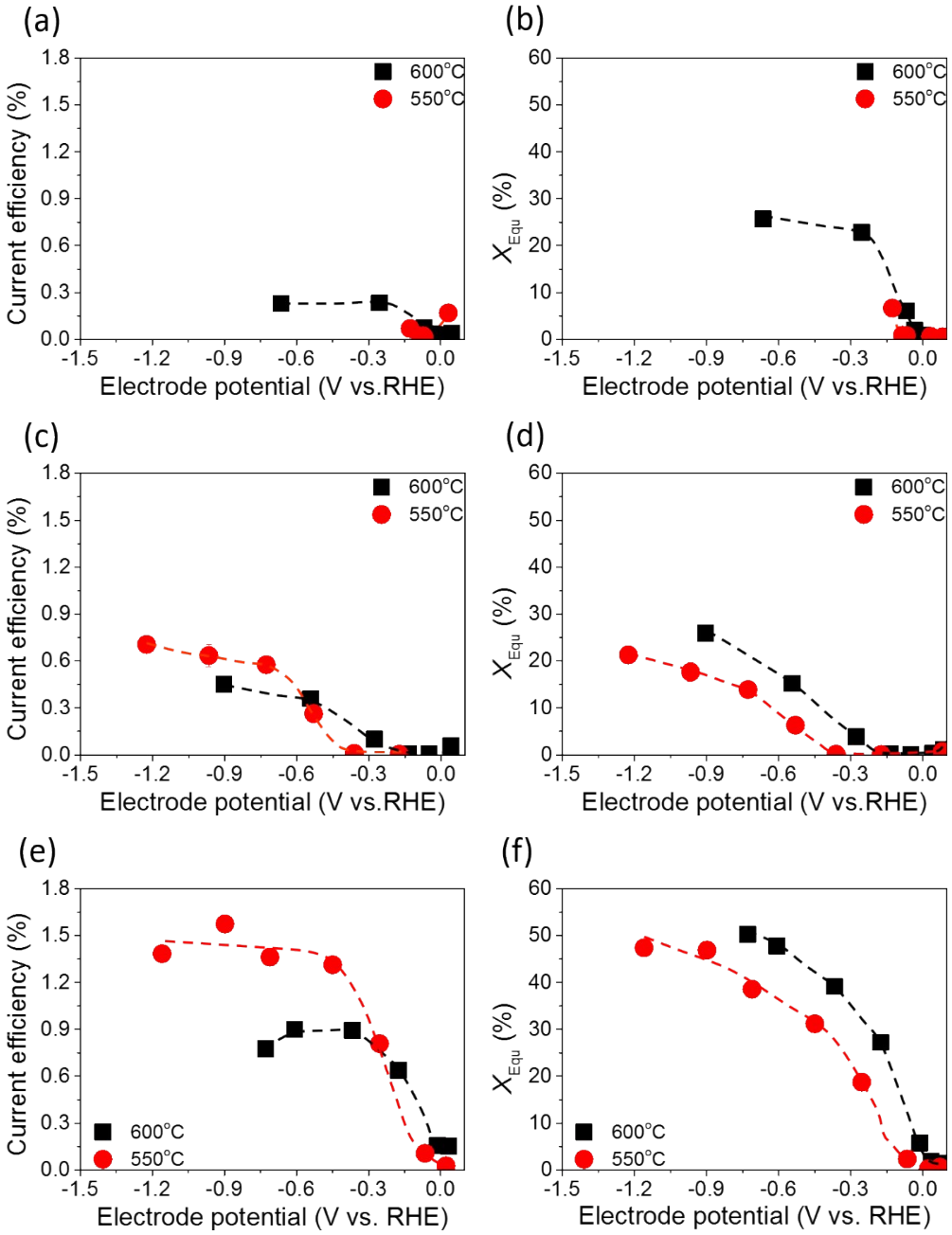

Fig. S3. Current efficiencies for (a) 10Fe–BCY (type A), (c) 0.5W–10Fe–BCY (type A'), and (e) porous pure Fe (type B) cathodes. Fraction of obtained NH_3 concentration to NH_3 concentration at equilibrium, X_{Equ}, for (b) 10Fe–BCY (type A), (d) 0.5W–10Fe–BCY (type A'), and (f) porous pure Fe (type B) cathodes at 10% H_2–90% N_2 (20 sccm).

4. Degradation test of ammonia formation rate with a porous pure Fe electrode

Figure S4 shows the influence of the degradation of the porous pure Fe cathode on the ammonia formation rate at 550°C. The first experiment was conducted using 20% H_2− 80% Ar, Pt |BCY| Fe, 50% H_2− 50% N_2 before the experiment of 75% H_2− 25% N_2 in Fig. 7. The second experiment was conducted 5% H_2− 95% Ar, Pt |BCY| Fe, 50% H_2− 50% N_2 after the experiment of 75% H_2−25% N_2 in Fig. 7 in the main text. The ammonia formation rate in the second round decreased by around 15% in comparison with that in the first round, which was probably caused by the degradation of the cathode.

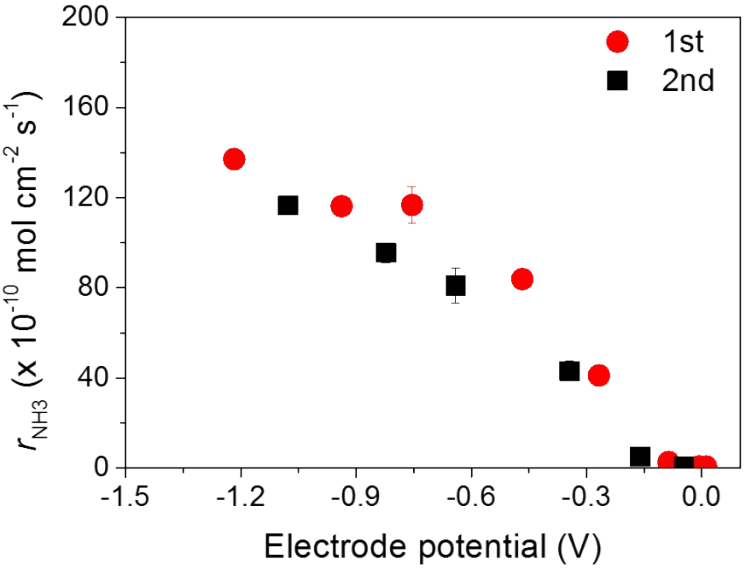

Fig. S4 The ammonia formation rate, r_{NH3}, in 50% H_2−50% N_2. The first experiment was conducted before the experiment in 75% H_2−25% N_2. The second round was held after the experiment in 75% H_2−25% N_2. Temp: 550°C.

5. The ammonia partial pressure p_{NH3} in the cathode and at equilibrium in different atmospheres

To understand difference between the amount of ammonia formed in the cathode and that at equilibrium, the ammonia partial pressure p_{NH3} in the cathode and that at equilibrium in different atmospheres were summarized in Table S1.

Table S1 Ammonia partial pressure p_{NH3} in the cathode and at equilibrium in different atmospheres (10^{-6} atm).

Applied voltage	10% H_2−90% N_2		25% H_2−75% N_2		50% H_2−50% N_2		75% H_2−25% N_2	
	p_{NH3} in the cathode	p_{NH3} at equilibrium	p_{NH3} in the cathode	p_{NH3} at equilibrium	p_{NH3} in the cathode	p_{NH3} at equilibrium	p_{NH3} in the cathode	p_{NH3} at equilibrium
Rest potential	0.06	73.8	0.50	266	0.90	614	0.29	797
-0.1	0.33	74.5	0.75	267	1.05	614	0.33	797
-0.3	16.1	75.0	16.5	268	3.82	615	1.08	797
-0.5	22.3	75.1	73.6	268	59.1	615	7.00	797
-0.7	25.5	75.1	84.5	268	121	615	51.2	797
-1.0	28.2	75.3	115	268	168	615	107	797
-1.2	29.2	75.3	105	268	16	615	137	797
-1.5	31.7	75.5	96.6	268	197	615	154	797

Table S2 Reaction rates and conditions of ammonia electrochemical synthesis

Cathode	Electrolyte	T (°C)	r_{NH3} (10^{-9} mol s^{-1} cm^{-2})	r_{NH3} (μg h^{-1} mg^{-1})	Flow rate (sccm)	X_{equ}	Atmosphere in the cathode	Atmosphere in the anode	Current efficiency (%)	Electrode surface area (cm^2)	Electrode weight (mg)	Electrode thickness (μm)	Ref.
Fe	BCY*1	550	13.7	450	40	32.1	50%H_2-50%N_2	20%H_2-80%Ar	14.5	0.39	0.7	12.5	This study
K-Al-Fe-BCY	BCY*1	650	0.7	4	20	32.0	15%H_2-85%N_2	20%H_2-80%Ar	0.3	0.39	0.33	30	1
BCZY-Ni	BCZY*2	620	2.9	1.7	150	79.1	50%H_2-50%N_2	50%H_2-50%N_2	3.3	1	750	–	2
Fe	SZY*3	450	1.1	2.2	50	2.8	75%H_2-25%N_2	H_2	200	2	62	–	3
Ag-Co_3Mo_3N	$LiAlO_2$-$(Li,Na,K)_2CO_3$	450	0.3	–	–	–	N_2	H_2	–	0.64	–	–	4
$Ru/Cs^+/MgO$*4	CsH_2PO_4/SiP_2O_7	250	12.4	116.8	1	–	N_2	Ar- H_2O	12	0.79	–	1500	5
VN	HCl	25	0.3	9.5	30	–	N_2	–	3.6	–	–	–	6
N doped Fe_3C	KOH	25	–	15.8	30	–	N_2	–	2.7	1	–	–	7
Fe-N-C	KOH	25	0.1	7.5	–	–	N_2	–	56.6	1	1	–	8
Co_3O_4	H_2SO_4	25	–	42.6	–	–	N_2	–	8.5	1	–	–	9

*1 $BaCe_{0.9}Y_{0.1}O_3$: BCY
*2 $BaCe_{0.2}Zr_{0.7}Y_{0.1}O_3$: BCZY
*3 $SrZr_{0.9}Y_{0.1}O_3$: SZY
*4 operating pressure was 0.7 MPa

6. Electrochemical ammonia synthesis in different atmospheres (pure N_2 and 10%H_2/90%N_2)

Figure S5 shows the influence of atmosphere in the cathode on ammonia formation rate. For the type A, the electrochemical promotion of ammonia formation was observed with cathodic polarization in a gaseous mixture of N_2–H_2 in the cathode. On the other hand, very low ammonia formation rate (3.3×10^{-12} – 1.7×10^{-11} mol cm^{-2} s^{-1}) was observed in pure N_2 even with an increase in the cathodic polarization for the type A cathode. If we assume the current efficiency of hydrogen evolution reaction is 100%, H_2 pressure in the cathode determined by the hydrogen evolution reaction is about 0.002 atm (0.2%). Therefore, H_2 in the cathode play an important role for ammonia formation, and the source of hydrogen in ammonia will originates from hydrogen supplied in the cathode rather than proton diffused from the anode to the cathode.

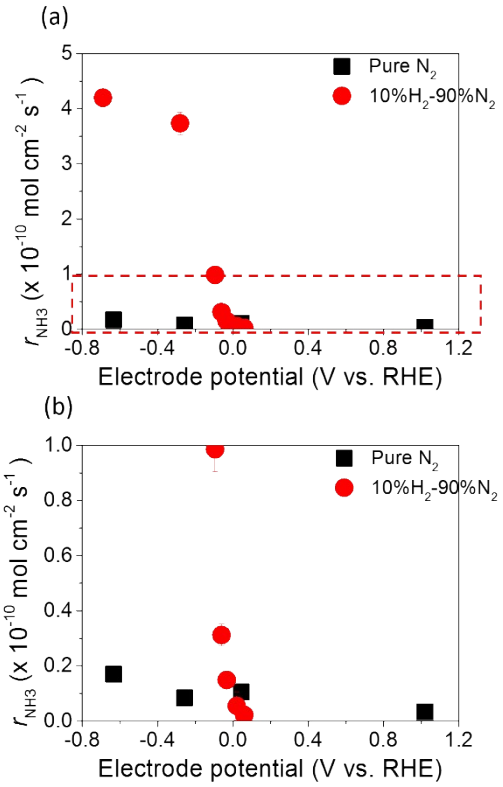

Fig. S5 (a) The performance of ammonia formation using 10Fe–BCY cathode at 600°C and pure N_2. (b) An enlarged view of the area surrounded by the red broken line in (a).

7. Electrochemical reaction of ammonia synthesis using Fe-yttria-stabilized zirconia (Fe-YSZ) cathode catalyst

YSZ pellet was prepared through the same process as the BCY pellet using YSZ powder (10%Y_2O_3, Tosoh, Co., Inc., Japan). YSZ porous cathode and 10Fe–YSZ (Fig. S6a) were also prepared by the same method as the BCY porous cathode and 10Fe–BCY.

Using the cell composed of 20%H_2-80%Ar, Pt |YSZ|10Fe-YSZ, 10%H_2-90%N_2, electrochemical promotion of the ammonia formation rate was not observed with cathodic polarization (Fig. S6b). Because YSZ is a pure oxide ion conductor, the result in Fig. S6b suggests that proton contributes to promoting ammonia formation rate and that the formation of the effective double layer with proton in the cathode plays an important role in the promotion of ammonia formation reaction as well as cathodic polarization (see the main text).

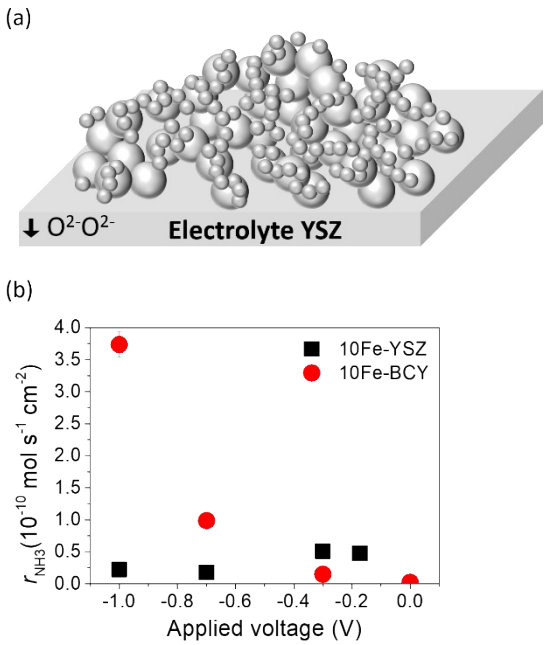

Fig. S6 (a) A schematic image of the 10Fe–YSZ electrode structure. (b) The performance of ammonia formation using 10Fe–YSZ cathode on YSZ electrolyte and 10Fe–BCY on BCY electrolyte at 600°C and 10% H_2–90% N_2.

8. Estimation of TPB length and Fe surface area in type A

We assume that the shape of Fe particles adsorbed on the BCY surface is semicircular, as shown in Fig. S7.

The surface area and TPB length are calculated by Eq. S1 and S2, respectively.

$$A_A = \frac{m_A}{\frac{4\pi}{3}\left(\frac{D_A}{2}\right)^3 \times d} \times \frac{4\pi\left(\frac{D_A}{2}\right)^2}{2} \quad \text{(S1)}$$

$$l_A = \frac{M_A}{\frac{4\pi}{3}\left(\frac{D_A}{2}\right)^3 \times d} \times \pi D_{A'} \quad \text{(S2)}$$

where A_A, m_A, D_A, l_A, and d were physical surface area, Fe weight in the cathode, Fe particle average diameter, total triple phase boundary length in type A, and Fe density (7.874 g^{-1} cm^{-3}). The average Fe particle size was calculated by the FE−SEM image of Fe particles in 10Fe−BCY after the electrochemical measurement (see Fig. 2i in the main text), as shown in Fig. S8. The resultant values of the TPB length in type A are summarized in Fig. S9 and Table S3.

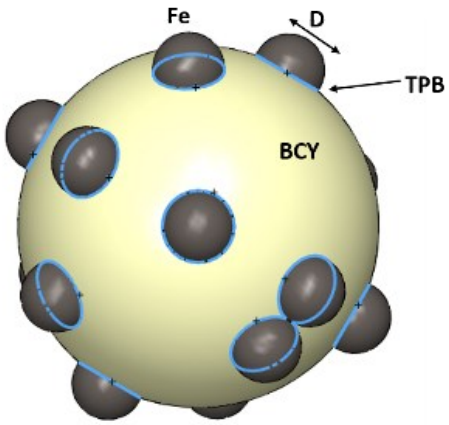

Fig. S7 A schematic image of the Fe–BCY structure for calculating the particle size, surface area, and triple-phase boundary.

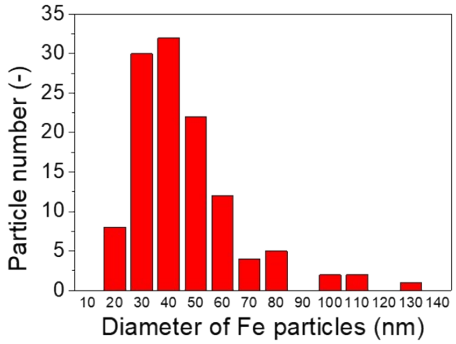

Fig. S8 The Fe particle size distribution in the type A.

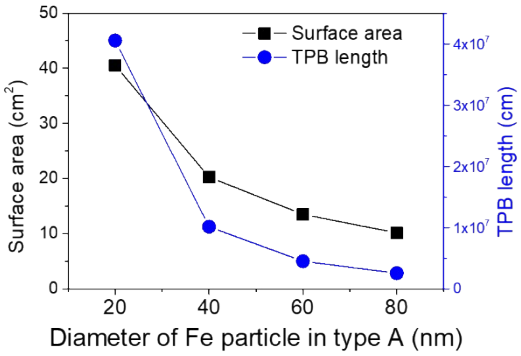

Fig. S9 Dependence of TPB length and surface area on Fe particle size in the type A.

Table S3 Fe particle size, surface area, TPB in type A*

m_A (mg)	Counted particle number (-)	D_A (nm)	S_A (cm^2)	l_A ($\times 10^6$ cm)
0.1	120	42 ± 25	19.1 ± 14.3	9.0 ± 5.3

* The errors in the table were estimated by the standard deviation.

9. Estimation of Fe surface area and TPB length in type B

The preparation of the type B electrode (pure porous Fe electrode) is as follows. First, the mixture of the slurry and Fe_2O_3 powder was pasted on the Al_2O_3 plate and annealed at 900°C in the air, and then the powder was reduced at 900°C in 3%H_2. Finally, the Fe powder was removed from the Al_2O_3 plate. The physical surface area, A_B, was estimated by the BET measurement, as shown in Fig. S10. The observed specific surface area (S_t) of Fe particles in type B was 0.71 m^2/g.

$$S_t = \frac{\frac{1}{m_{BET} + I_{BET}} \times N_A \times \sigma}{M} \quad \text{(S3)}$$

where m_{BET}, I_{BET}, N_A, σ, M are the slope and intercept in the BET measurement, Avogadro's number, the adsorption cross section of the adsorbing species, and the molecule weight of the adsorbate gas.

Considering the weight of Fe electrode, the resultant value of A_B was 5 cm^2. To estimate TPB length in type B, l_B, the average Fe particle size was determined by the FE-SEM image of Fe particles in porous pure Fe after the electrochemical measurement (Fig. 2k), as shown in Fig. S11. Then, we assume that Fe particles accumulate to form a columnar structure, as shown in Fig. S12. Therefore, the porosity of the cathode is the same as the coverage of Fe particles on the BCY electrolyte. The TPB region is the interface between the Fe column and BCY electrolyte, which is calculated by Eq. S4.

The TPB length is summarized in Fig. S13. The resultant values are summarized in Table S4.

$$l_B = \frac{A_{ele} \times (1-\varphi)}{\pi \times (\frac{D_B}{2})^2} \times \pi D_B \quad \text{(S4)}$$

where l_B, φ, D_B, and A_{ele} were triple phase boundary length, porosity, Fe particle average diameter in type B, and the area of the electrode, which is a semi-circle with 10 mm diameter.

$$A_{ele} = \frac{\pi \times (\frac{D_{ele}}{2})^2}{2} \quad \text{(S5)}$$

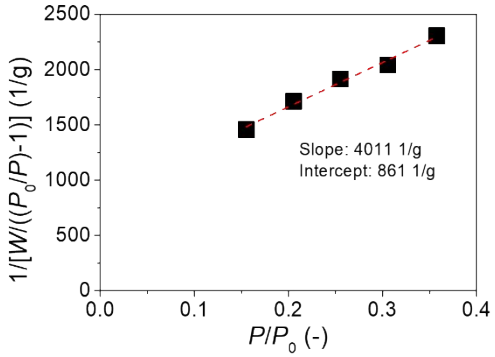

Fig. S10 BET measurement for the type B porous pure Fe.

where D_{ele} is diameter of electrode (10 mm).

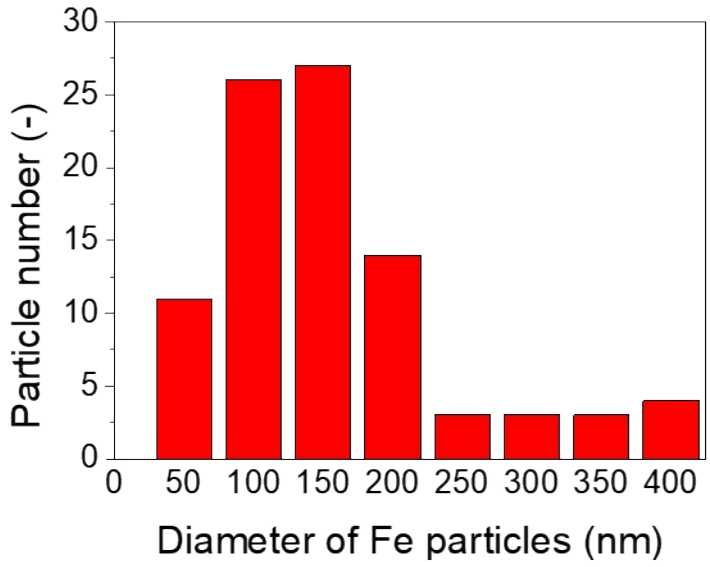

Fig. S11 The Fe particle size distribution in the type B.

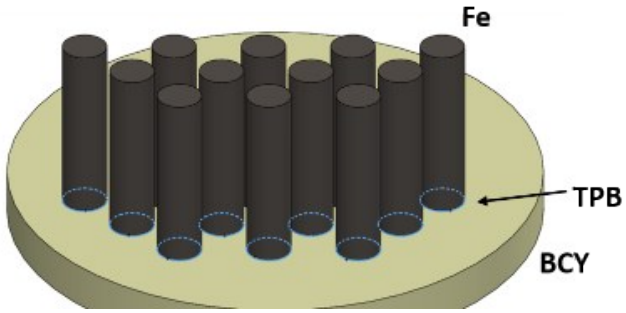

Fig. S12 A schematic image of porous pure Fe structure to calculate the triple phase boundary.

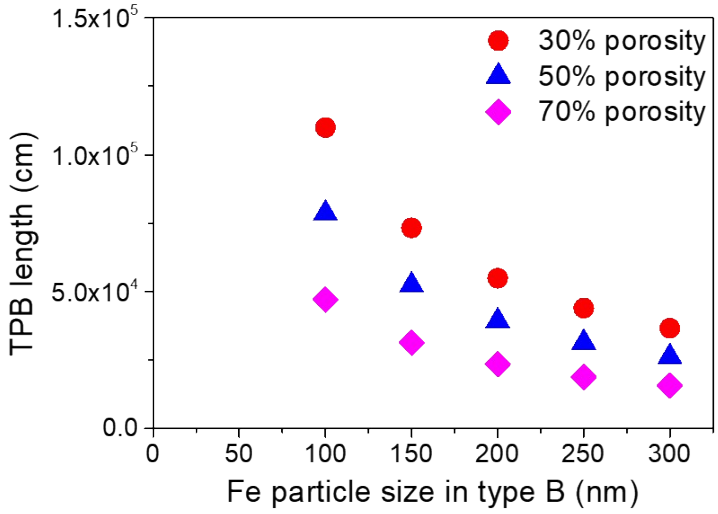

Fig. S13 The TPB length vs. Fe particle size in the type B.

Table S4 Fe Particle size and triple phase boundary of Fe in type B porous pure Fe electrode*

$m_{B\square}$(mg)	Counted particle number (-)	$D_{B\square}$(nm)	$A_{B\ \square}$ (cm^2)	l_B ($\times 10^4$ cm)
0.7	91	190 ± 108	5.0	5.8 ± 3.3

* The errors in the table were estimated by the standard deviation.

10. Estimation of the area of the effective surface area (S_i)

・ In type A, the volume ratio of Fe particles having a network structure of electrons to all Fe particles is low (1.0%).

・ Although the effective TPB length in type A is longer than that in type B, the area of the effective surface area in type A is smaller than that in type B.

The details of the estimations are as follows.

The area of the effective surface area and effective double layer are discussed in section 10 and 11, respectively. To calculate the area of the effective surface area in section 10, we use the following parameters stated below:

l_i (i = A or B): TPB length, which is already shown in Table S3 for type A and Table S4 for type B in the sections 8 and 9.

$l_{eff,i}$ (i = A or B): effective TPB length, which is determined by Fe particles connected with a network structure of electrons.

A_i (i = A or B): physical surface area, i.e. total surface area, of Fe particles, as already shown in Table S3 for type A and Table S4 for type B in the sections 8 and 9.

S_i (i = A or B): effective surface area of Fe particles, i.e. Fe particles connected with a network structure of electrons, as shown in Fig. S14.

The ammonia formation rate in type B was higher than that in type A, but type B had a smaller physical surface area for Fe particles than type A (see Tables S3 and S4). The reason is that the ammonia formation cannot be promoted via isolated Fe particles that disconnected from the network structure in type A with cathodic polarization (Fig. S14).

To calculate S_A, we assume that current density, i.e., proton flux, is proportional to the effective TPB length, l_{eff}. Although the TPB length in type A was 243 times longer than that in type B (Table S4), the current density in type A of 10Fe–BCY was just 1.6 times higher than that in type B of pure porous Fe at 600°C, as discussed in the main text (Fig. 5). This discrepancy is probably caused by that a part of the Fe particles on BCY surface in type A do not work for the charge-transfer reaction and do not connect with a network structure (i.e. isolated Fe particles exist on BCY surface in type A, as shown in Fig. S14), which suggests that A_A is not equal to S_a ($A_A \neq S_A$), and l_A is not equal to $l_{eff,A}$ as well ($l_A \neq l_{eff,A}$). As for type B, because of the assumption that the all Fe particles in type B connect with a network structure ($A_B = S_B$), $l_{eff,B}$ is the same as total TPB length in type B, l_B, ($l_B = l_{eff,B}$). Therefore, $l_{eff,A}$ can be obtained by Eq. S6, assuming that the current density is proportional to the effective TPB length. Then, S_A can be obtained by Eq. S7.

$$\frac{i_A}{i_B} = \frac{l_{eff,A}}{l_{eff,B}} \tag{S6}$$

$$\frac{l_A}{A_A} = \frac{l_{eff,A}}{S_A} \quad \text{(S7)}$$

where i_A and i_B, are the current densities at 600°C using type A and type B, respectively; $l_{eff,A}$ and $l_{eff,B}$ are the effective TPB lengths in type A and type B, respectively; and l_A, A_A, and S_A are total TPB length, physical surface area (total surface area), and effective surface area in type A, respectively.

The volume ratio of Fe particles having a network structure of electron is dependent on the parameters of Fe particle sizes in 10Fe-BCY (20 nm ~ 80 nm), porous pure Fe (100 nm ~ 300 nm), and porosity in porous pure Fe (30 ~ 70%), as shown in Fig. S15. If we consider that the average value of the size of Fe particles are 42 and 190 nm in type A and type B, respectively, the volume ratio of Fe particles having a network structure of electron is around 1.0% in the porosity of 30%. The effective surface area of Fe particles in type A, S_A was around 0.18 cm^2, and that of type B, S_B, was 5 cm^2 by the BET measurement.

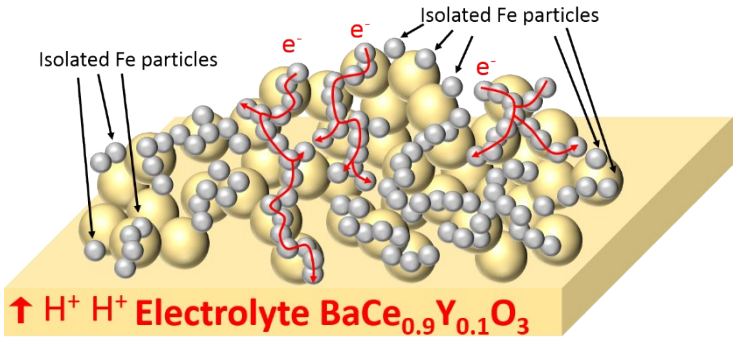

Fig. S14 A schematic image of Fe particles connected with a network structure and isolated Fe particles in type A.

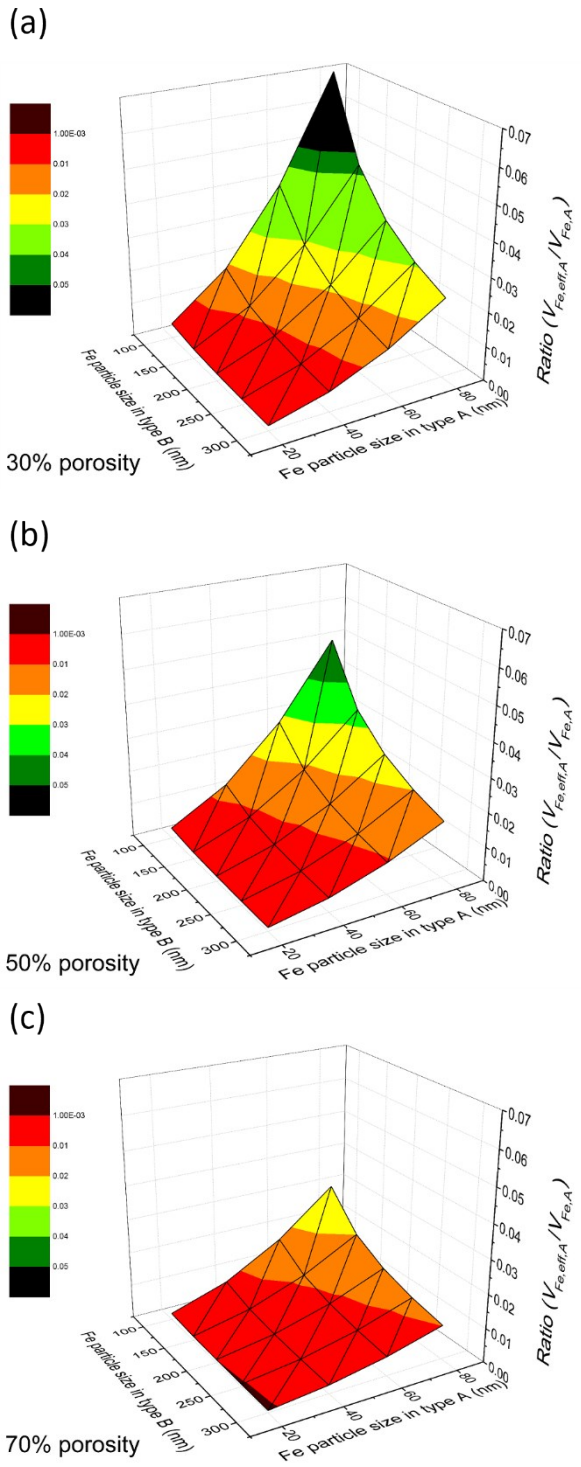

Fig. S15 The ratio of the volume of Fe particles with network structure of electron to the volume of Fe isolated particles vs. Fe particle size in the type A and type B with (a) 30% porosity, (b) 50% porosity, and (c) 70% porosity in the type B, respectively.

11. Estimation of the area of the effective double layer ($S^*_{eff,i}$)

・ The area of effective double layer in type A and type B are 0.20 and 0.41 cm^2, respectively.

・ The proton diffusion length in type B is around 1.03 μm, which is much less than the electrode thickness.

The details of the estimations are as follows.

To calculate the area of the effective double layer in section 12, we use the following parameters stated below:

$S^*_{eff,i}$ (i = A or B): the area of effective double layer, which was covered by protons on S_A or S_B, for promoting N_2 dissociation and subsequent ammonia formation, as shown in Fig. S16.

The effective double layer can be formed via H^+ spillover on the Fe particle surface that connected with the network structure, as shown in Fig. S16. The area of the effective double layer is the reaction area for ammonia formation. Because of the small diameter of several tens nanometers for Fe particles, protons diffused from the electrolyte can cover the whole Fe surface via diffusion in type A (Fig S16 and Fig. 9b in the main text). However, in type B, proton diffusion length is too short to reach the top of the Fe electrode from the electrolyte because the Fe electrode is thick, 12.5 μm

(see Fig. S2d). Therefore, the effective double layer will be formed in a part of the porous pure Fe cathode. Here, we introduce a new parameter, proton diffusion length, *h*, which should be shorter than the thickness of the electrode, *H* (12.5 μm), in type B, as shown in Fig. 9c in the main text. The relation between *h* and *H* could be represented by Eq. S8:

$$h = H \times \tau \tag{S8}$$

where τ is a constant between 0 and 1. Therefore, we assume that the area of the effective double layer $S^*_{\mathrm{eff,A}}$ is equal to the effective surface of Fe particles in type A, as described by Eq. S9. In type B, the area of the effective double layer $S^*_{\mathrm{eff,B}}$ can be changed by the effective surface area of the Fe particles multiplied by τ, as described in Eq. S10.

$$S^*_{eff,A} = S_A \tag{S9}$$

$$S^*_{eff,B} = S_B \times \tau \tag{S10}$$

Because the operating temperature and atmosphere in the electrochemical reaction for ammonia formation were the same for type A and type B, we assume that the ammonia formation rate is proportional to the reaction area/effective double layer, as described by Eq. S11:

$$\left(\frac{r_{NH3,A}}{r_{NH3,B}}\right) = \frac{\left(S^*_{eff,A}\right)}{\left(S^*_{eff,B}\right)} = \frac{(S_A)}{(S_B \times \tau)} \tag{S11}$$

As a result, τ is estimated to be 0.01−0.30 and the proton diffusion length h is about sub-micrometer to several micrometers for the type B, as shown in Fig. S17. If we consider that the average value of the size of Fe particles are 42 and 190 nm in type A and type B, respectively, the value of τ and the proton diffusion length are about 0.08 and 1.03 μm in the porosity of 30%, respectively, as summarized in Table S5.

Table S5 Estimation of the proton diffusion length and relevant parameters in the porosity of 30%.

	D_{av} (cm)	$S^*_{eff,I}$ (cm^2)*	h (μm)*	τ (-)*
Type A	42 ± 25	0.20 ± 0.02	-	-
Type B	190 ± 108	0.41 ± 0.04	1.03 ± 0.11	0.08 ± 0.01

* The errors were estimated by the standard error.

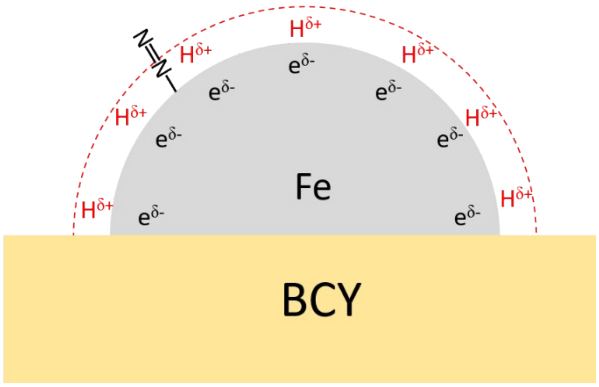

Fig. S16 A schematic image of effective double layer formation on Fe

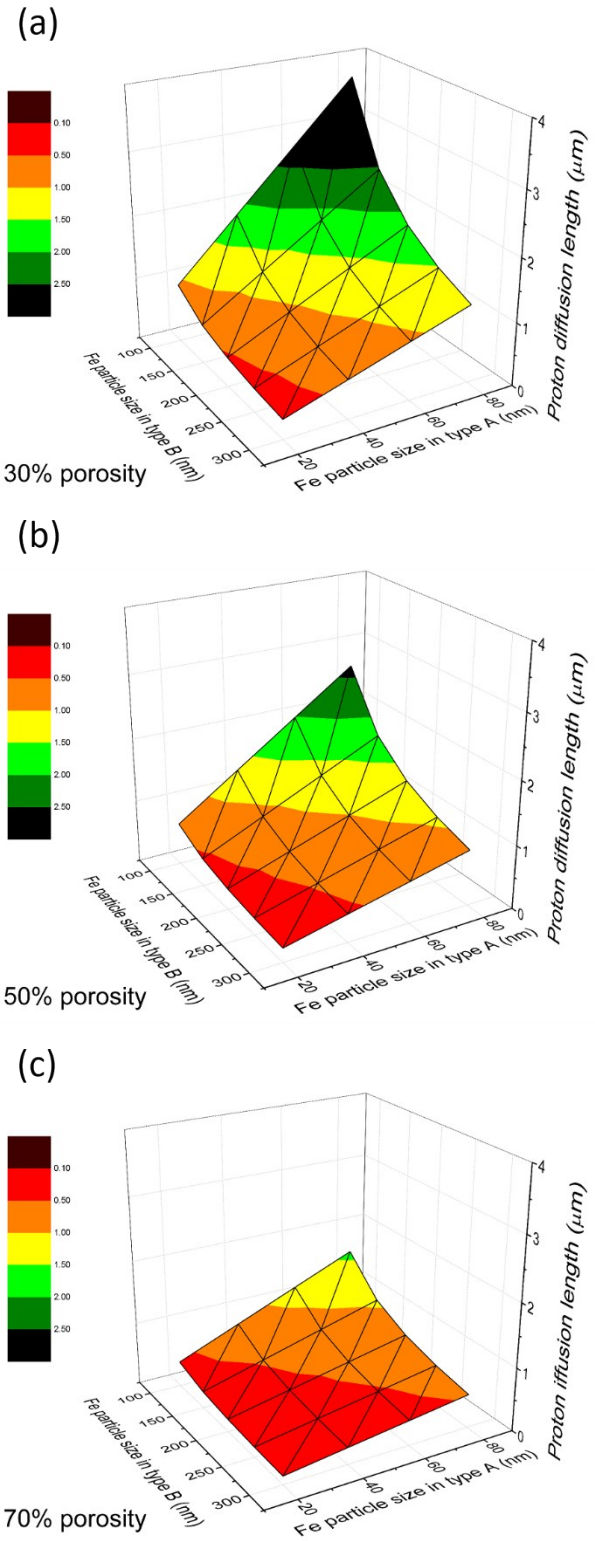

Fig. S17 Proton diffusion length vs. Fe particle size in the type A and type B with (a) 30% porosity, (b) 50% porosity, and (c) 70% porosity in the type B, respectively.

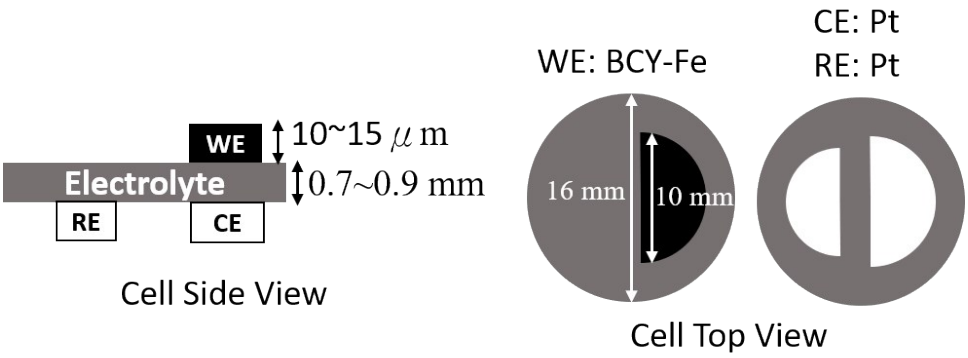

Fig. S18 Schematic images of a single cell.

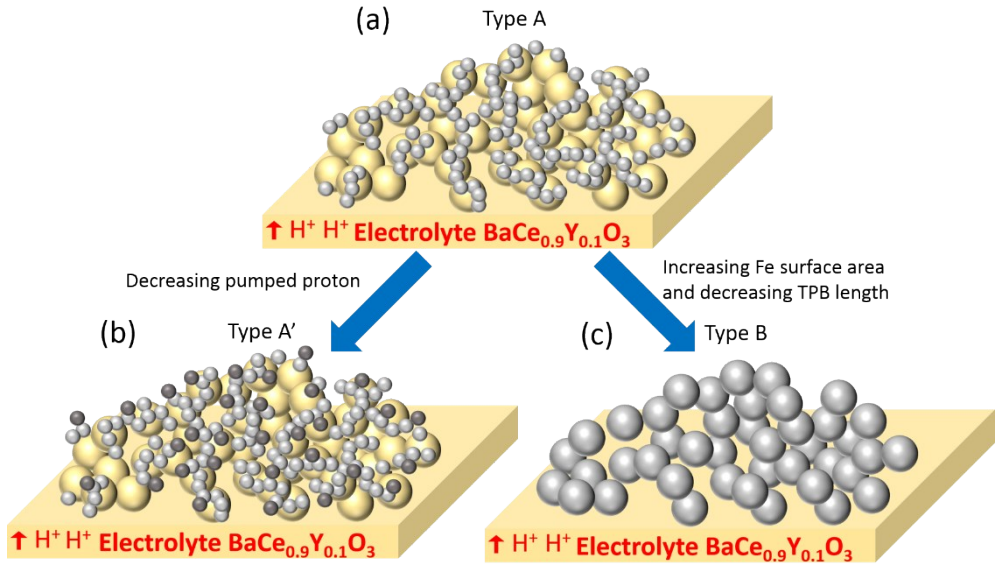

Fig. S19 Schematic images of cathode structures of (a) Fe–BCY, (b) W–Fe–BCY cathodes, and (c) porous pure Fe.

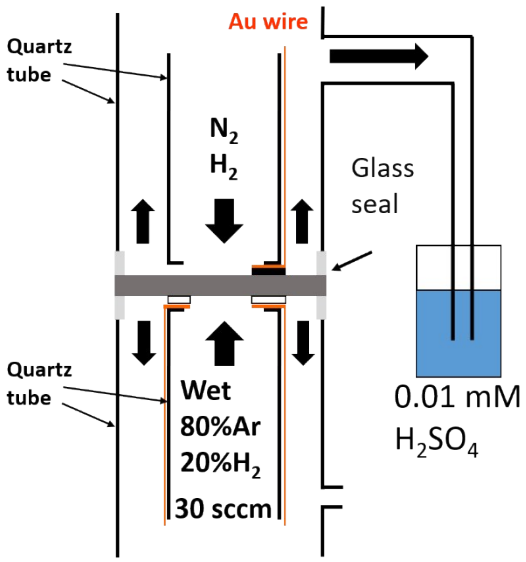

Fig. S20 A schematic image of device for electrochemical synthesis of ammonia.

12. The current efficiency for hydrogen pumping

Figure S21 shows that the current efficiency for the hydrogen evolution reaction using a single cell of 20% H_2−80% Ar, Pt |BCY| porous pure Fe, Ar with the three-electrodes method. The current efficiencies for hydrogen evolution reaction were around 80-85% at electrode potentials between 0.085 V and 0.052 V (corresponding applied voltages between −0.2 V and −0.35 V). The main reason for the loss will be caused by the leakage current, which is induced by hole and/or electron conduction through the electrolyte membrane. The electrochemical reaction of ammonia formation includes the electrochemical synthesis of ammonia and hydrogen evolution reaction in parallel. The typical current efficiency for NH_3 formation is below 2% in this study, which indicated that the pumped protons tend to form H_2 rather than NH_3. The result suggests that the hydrogen evolution reaction is dominant in the electrochemical reaction.

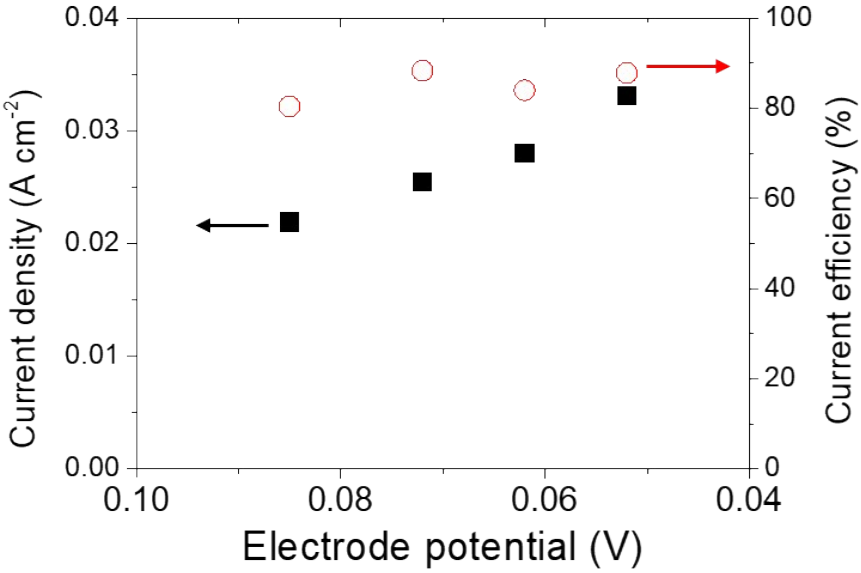

Fig. S21 Current efficiency using the cell of 20% H_2−80% Ar, Pt |BCY| Fe, Ar.

13. Blank test for ammonia electrosynthesis

A blank test without N_2 supply was conducted with changing electrode potential in a gaseous mixture of 10% H_2–90% Ar, which was supplied into the cathode (Fig. S22). A low ammonia formation rate of around 2×10^{-12} mol cm^{-2} s^{-1} was observed. In our equipment, the detection limit of ammonia formation rate was around 2×10^{-12} mol cm^{-2} s^{-1}. Therefore, we concluded almost no ammonia formation under the standard condition of 10% H_2–90% Ar at 550°C.

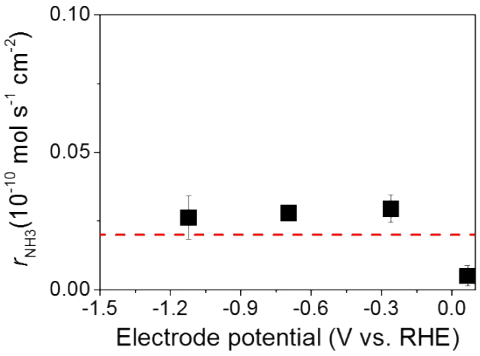

Fig. S22 Blank test of ammonia formation using porous pure Fe cathode at 550°C in 10% H_2–90% Ar. The red broken line is the detection limit of HPLC.

14. Ammonia decomposition reaction test

To understand the influence of the device (cell and quartz tube) and the cathode on ammonia decomposing into N_2 and H_2, the ammonia decomposition reaction test of NH_3 was conducted using an Al_2O_3 plate (i.e., a dummy cell without the cathode) and a single cell with porous pure Fe electrode, as shown in Fig. S23a and S23b, respectively.

First, 50 ppm NH_3–5% D_2–45% Ar–50% N_2 balanced gaseous mixture was directly captured with a 0.01 mM H_2SO_4 solution at ambient temperature and introduced into the device using the Al_2O_3 plate. The ammonia concentration at 600°C was mostly the same as that at ambient temperature. These results demonstrated that ammonia could not decompose on the quartz tube or the Al_2O_3 plate below 600°C, as shown in Fig. S23a.

Second, the flowing gas was changed to 100 ppm NH_3–N_2 balanced gaseous mixture and introduced into the device with a single cell with porous pure Fe electrode. The detected ammonia concentration was 81 ppm, which suggested that a part of ammonia was adsorbed on the gas tube surface. Subsequently, 100 ppm NH_3–N_2 balanced gaseous mixture was introduced into the cathode and captured at 500°C–600°C using the 0.01 mM H_2SO_4 solution. The detected ammonia concentrations were

25 ppm at 600°C and 50 ppm at 500°C. These results suggest that the reverse reaction of NH_3 occurred on the Fe electrode below 600°C.

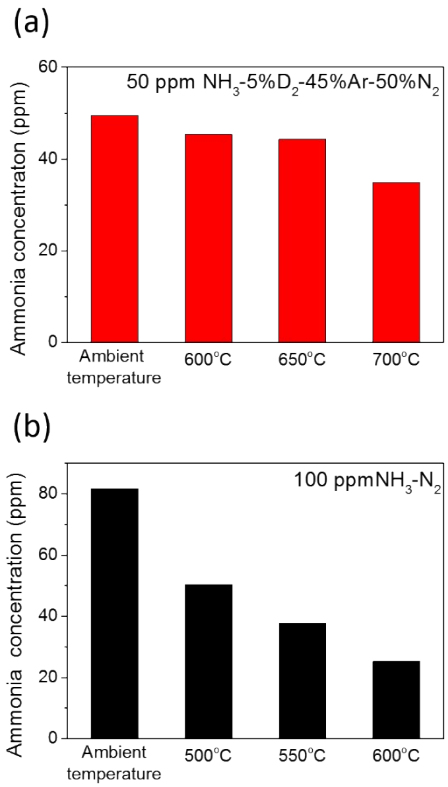

Fig. S23 The ammonia decomposition reaction test using (a) Al_2O_3 plate at 50 ppm NH_3–5% D_2–45% Ar–50% N_2 and (b) porous pure Fe cathode at 100 ppm NH_3–N_2.

15. Reversible test for ammonia electrochemical synthesis

A reversible test with forward and reverse changes of electrode potential was conducted for ammonia electrochemical synthesis at 550°C in 10% H_2–90% N_2 gaseous mixture. The ammonia formation rate in Fig. S24 shows reversible behavior with cathodic polarization. These results suggest that the promotion of ammonia formation rate in this study was caused by cathodic polarization (EPOC) and not just by the reduction of the Fe electrode itself.

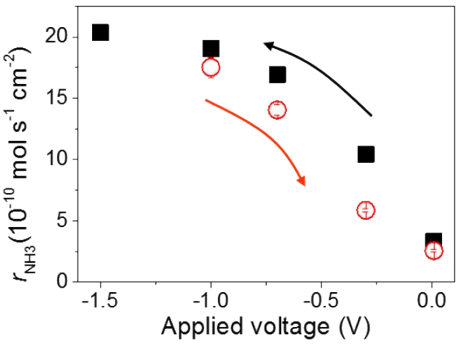

Fig. S24 Electrochemically reversible test for ammonia formation rate using porous pure Fe (30 μm) at 550°C and 10% H_2–90% N_2 (40 sccm).

16. Stability for ammonia electrochemical synthesis

The stability test was performed using the cell of wet 20% H_2−80% Ar, Pt |BCY| Fe, 10% H_2−90% N_2 at −1V and 550°C, as shown in Fig. S25. The stable ammonia formation rate of around 1.7×10^{-9} mol cm^{-2} s^{-1} was observed for 12 hours.

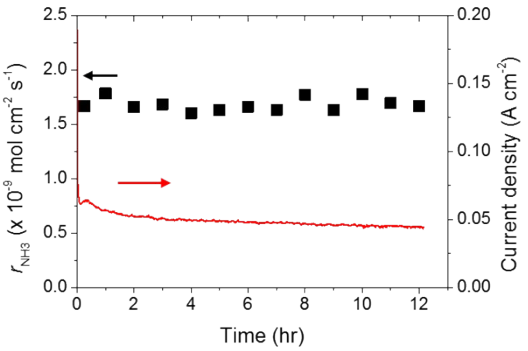

Fig. S25 Stability test using the cell of wet 20% H_2−80% Ar, Pt |BCY| Fe, 10% H_2−90% N_2 at −1 V and 550°C.

17. References

1. F. Kosaka, T. Nakamura, A. Oikawa, and J. Otomo, *ACS Sustainable Chemistry & Engineering,* **5** (11), 10439-10446 (2017).
2. E. Vasileiou, V. Kyriakou, I. Garagounis, A. Vourros, A. Manerbino, and M. Stoukides, *Solid State Ionics,* **275** 110-116 (2015).
3. M. Ouzounidou, A. Skodra, C. Kokkofitis, and M. Stoukides, *Solid State Ionics,* **178** (1-2), 153-159 (2007).
4. I. A. Amar, R. Lan, C. T. G. Petit, and S. Tao, *Electrocatalysis,* **6** (3), 286-294 (2014).
5. K. Imamura and J. Kubota, *Sustainable Energy & Fuels,* **3** (6), 1406-1417 (2019).
6. X. Zhang, R. M. Kong, H. Du, L. Xia, and F. Qu, *Chemical communications,* **54** (42), 5323-5325 (2018).
7. L. Cong, Z. Yu, F. Liu, and W. Huang, *Catalysis Science & Technology,* **9** (5), 1208-1214 (2019).
8. M. Wang, S. Liu, T. Qian, J. Liu, J. Zhou, H. Ji, J. Xiong, J. Zhong, and C. Yan, *Nature communications,* **10** (1), 341 (2019).
9. S. Luo, X. Li, B. Zhang, Z. Luo, and M. Luo, *ACS applied materials & interfaces,* **11** (30), 26891-26897 (2019).